HHS Public Access

Author manuscript

Angew Chem Int Ed Engl. Author manuscript; available in PMC 2016 December 05.

Published in final edited form as:

Angew Chem Int Ed Engl. 2016 December 5; 55(49): 15297–15300. doi:10.1002/anie.201608338.

Magneto-Plasmonic Janus Vesicles for Magnetic Field-Enhanced Photoacoustic and Magnetic Resonance Imaging of Tumors

Dr. Yijing Liu,
Department of Chemistry and Biochemistry, University of Maryland, College Park, MD, 20742 (USA). Laboratory of Molecular Imaging and Nanomedicine (LOMIN), National Institute of Biomedical Imaging and Bioengineering (NIBIB), National Institutes of Health (USA) and Trans-NIH Shared Resource on Biomedical Engineering and Physical Science (BEPS), National Institute of Biomedical Imaging and Bioengineering (NIBIB), National Institutes of Health (USA)

Xiangyu Yang,
Laboratory of Molecular Imaging and Nanomedicine (LOMIN), National Institute of Biomedical Imaging and Bioengineering (NIBIB), National Institutes of Health (USA) and Trans-NIH Shared Resource on Biomedical Engineering and Physical Science (BEPS), National Institute of Biomedical Imaging and Bioengineering (NIBIB), National Institutes of Health (USA)

Zhiqi Huang,
Department of Chemistry and Biochemistry, University of Maryland, College Park, MD, 20742 (USA)

Prof. Peng Huang,
Guangdong Key Laboratory for Biomedical Measurements and Ultrasound Imaging, School of Biomedical Engineering, Shenzhen University, Shenzhen 518060 (P.R. China)

Yang Zhang,
Smart Hybrid Materials (SHMs) Lab Department of Chemical Sciences and Engineering, Advanced Membranes and Porous Materials Center, King Abdullah University of Science and Technology (KAUST), Thuwal 23955-6900 (Kingdom of Saudi Arabia)

Dr. Lin Deng,
Smart Hybrid Materials (SHMs) Lab Department of Chemical Sciences and Engineering, Advanced Membranes and Porous Materials Center, King Abdullah University of Science and Technology (KAUST), Thuwal 23955-6900 (Kingdom of Saudi Arabia)

Zhantong Wang,
Laboratory of Molecular Imaging and Nanomedicine (LOMIN), National Institute of Biomedical Imaging and Bioengineering (NIBIB), National Institutes of Health (USA) and Trans-NIH Shared Resource on Biomedical Engineering and Physical Science (BEPS), National Institute of Biomedical Imaging and Bioengineering (NIBIB), National Institutes of Health (USA)

Zijian Zhou,

Correspondence to: Niveen M. Khachab, niveen.khashab@kaust.edu.sa; Xiaoyuan Chen, shawn.chen@nih.gov; Zhihong Nie, znie@umd.edu.

Supporting information and the ORCID identification number(s) for the author(s) of this article can be found under http://dx.doi.org/10.1002/anie.201608338.

Laboratory of Molecular Imaging and Nanomedicine (LOMIN), National Institute of Biomedical Imaging and Bioengineering (NIBIB), National Institutes of Health (USA) and Trans-NIH Shared Resource on Biomedical Engineering and Physical Science (BEPS), National Institute of Biomedical Imaging and Bioengineering (NIBIB), National Institutes of Health (USA)

Dr. Yi Liu,
Department of Chemistry and Biochemistry, University of Maryland, College Park, MD, 20742 (USA)

Dr. Heather Kalish,
Laboratory of Molecular Imaging and Nanomedicine (LOMIN), National Institute of Biomedical Imaging and Bioengineering (NIBIB), National Institutes of Health (USA) and Trans-NIH Shared Resource on Biomedical Engineering and Physical Science (BEPS), National Institute of Biomedical Imaging and Bioengineering (NIBIB), National Institutes of Health (USA)

Prof. Niveen M. Khachab,
Smart Hybrid Materials (SHMs) Lab Department of Chemical Sciences and Engineering, Advanced Membranes and Porous Materials Center, King Abdullah University of Science and Technology (KAUST), Thuwal 23955-6900 (Kingdom of Saudi Arabia)

Dr. Xiaoyuan Chen, and
Laboratory of Molecular Imaging and Nanomedicine (LOMIN), National Institute of Biomedical Imaging and Bioengineering (NIBIB), National Institutes of Health (USA) and Trans-NIH Shared Resource on Biomedical Engineering and Physical Science (BEPS), National Institute of Biomedical Imaging and Bioengineering (NIBIB), National Institutes of Health (USA)

Prof. Zhihong Nie
Department of Chemistry and Biochemistry, University of Maryland, College Park, MD, 20742 (USA)

Niveen M. Khachab: niveen.khashab@kaust.edu.sa; Xiaoyuan Chen: shawn.chen@nih.gov; Zhihong Nie: znie@umd.edu

Abstract

Magneto-plasmonic Janus vesicles (JVs) integrated with gold nanoparticles (AuNPs) and magnetic NPs (MNPs) were prepared asymmetrically in the membrane for in vivo cancer imaging. The hybrid JVs were produced by coassembling a mixture of hydrophobic MNPs, free amphiphilic block copolymers (BCPs), and AuNPs tethered with amphiphilic BCPs. Depending on the size and content of NPs, the JVs acquired spherical or hemispherical shapes. Among them, hemispherical JVs containing 50 nm AuNPs and 15 nm MNPs showed a strong absorption in the near-infrared (NIR) window and enhanced the transverse relaxation (T_2) contrast effect, as a result of the ordering and dense packing of AuNPs and MNPs in the membrane. The magneto-plasmonic JVs were used as drug delivery vehicles, from which the release of a payload can be triggered by NIR light and the release rate can be modulated by a magnetic field. Moreover, the JVs were applied as imaging agents for in vivo bimodal photoacoustic (PA) and magnetic resonance (MR) imaging of tumors by intravenous injection. With an external magnetic field, the accumulation of the JVs in tumors was significantly increased, leading to a signal enhancement of approximately 2–3 times in the PA and MR imaging, compared with control groups without a magnetic field.

Graphical Abstract

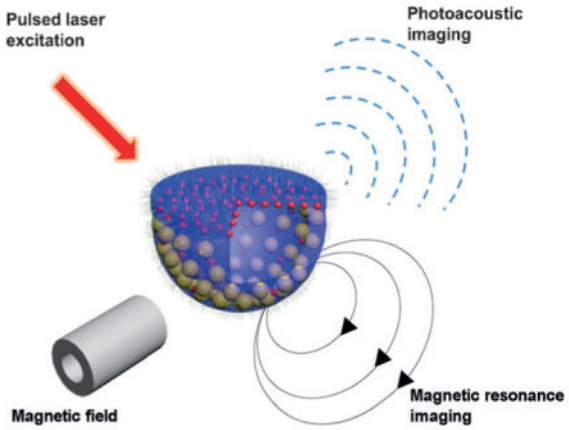

Magneto-plasmonic Janus vesicles, with controlled shape and nanoparticle organization in the membrane, were prepared by coassembly of amphiphilic block copolymers (~). The copolymers were subsequently tethered to gold (●) and magnetic (●) nanoparticles. The Janus vesicles allowed for magnetic field-enhanced bimodal photoacoustic and magnetic resonance imaging, as well as magnetic manipulation and near-infrared light triggered release of therapeutic agents.

Keywords

Janus vesicles; magnetic resonance imaging; nanoparticles; photoacoustic imaging; self-assembly

Inorganic nanoparticles (NPs) have shown promising applications in the treatment, diagnosis, and detection of many diseases because of their unique optical or magnetic properties.[1] For this purpose, single NPs are often functionalized with organic or polymeric ligands, to improve their stability, biocompatibility, and targeted delivery of therapeutic agents.[2] While single NPs are attractive, NP assemblies can exhibit new or advanced properties that are different from that of their individual counterparts, thus facilitating use in biomedical applications.[1f,3] A typical example is vesicular structures containing both NPs and polymers in the membrane. For example, vesicular assemblies of AuNPs can be used for effective encapsulation of therapeutic agents, near-infrared (NIR) light-triggered release of a payload, and multimodality imaging of cancers.[4] Embedding of MNPs in polymeric vesicular membranes increases the stability and biocompatibility of MNPs in a physiological environment. Moreover, the presence of many MNPs within individual assemblies increases their responsiveness to an external magnetic field and transverse relaxivity (r_2).[2b,5] Strong magnetic responsiveness promotes accumulation of NPs in tumors on application of a magnetic field, thus overcoming the limitation of tumor heterogeneity on passive tumor accumulation of NPs.[6] We hypothesize that integration of both AuNPs and MNPs in vesicles with controlled NP organization will further increase the functionalities of hybrid vesicles and hence broaden their potential biomedical applications.[4d,7]

Herein, we report the design of hybrid Janus-like vesicles (JVs) with controlled distribution of both AuNPs and MNPs in the vesicular membrane for effective bimodal imaging of

cancers. The magneto-plasmonic JVs were fabricated by coassembling a mixture of hydrophobic Fe_3O_4 MNPs, amphiphilic block copolymer (BCP) of polystyrene-*b*-poly(acrylic acid) (PS-*b*-PAA), and AuNPs grafted with polystyrene-*b*-poly (ethylene oxide) (PS-*b*-PEO) on the surface (Figure 1a). Depending on the size and mass fraction of NPs in the mixture, the assembly process produced spherical JVs (Figure 1b) or hemispherical JVs (Figure 1c). The hemispherical JVs containing 50 nm AuNPs and 15 nm MNPs exhibit a higher transverse relaxivity (r_2) value than individual MNPs and spherical JVs because of magnetic interactions between the MNPs within individual assemblies. Moreover, they show a strong absorption in the NIR range because of the plasmonic coupling between neighboring AuNPs densely packed within one half of the vesicular membrane. We demonstrated that model drugs can be encapsulated in the JVs and the release of the payload can be triggered by NIR laser irradiation. Furthermore, with an external magnetic field, the JVs can be enriched in the tumor upon intravenous injection, leading to an approximately two to three times enhancement in signal for PA and MR imaging of cancers, compared with that of control groups without an external magnetic field.

Two different sized hydrophobic Fe_3O_4 MNPs (25 nm and 15 nm), stabilized by oleic acid, are described herein.[8] BCP-tethered AuNPs were made by attaching thiol terminated PS_{490}-*b*-PEO_{45} onto the surfaces of NPs of different sizes (20 nm, 30 nm, and 50 nm; Supporting Information, Figure S1). BCPs of PS_{107}-*b*-PAA_4 without thiol groups were used as free BCPs. The self-assembly of a ternary mixture was triggered by a solvent exchange method (see the Supporting Information for experimental details).[9] Depending on the size and mass fraction of NP building blocks, the assembly process produced spherical and hemispherical JVs with two distinct halves, and homogenous vesicles (HVs) with uniform distributions of two types of NPs (Figure 2; Supporting Information, Figures S2 and S3). All JVs consist of a hollow cavity and a membrane composed of BCP-tethered AuNPs, MNPs, and free BCPs, as indicated by the higher contrast at the edges and the wrinkle surface—which are two characteristics typical of vesicles—of the assemblies displayed in the TEM images (Figure 2a,b; Supporting Information, Figure S2b).[10] The average diameter of the JVs was 570.8 ± 93.2 nm, characterized by dynamic light scattering (Supporting Information, Figure S4). Within the vesicular membranes of JVs, the BCP-tethered AuNPs were segregated and densely packed in one half of the vesicular membrane, while the hydrophobic MNPs could be clearly observed in the polymeric domains in another half of the vesicles. Close inspection revealed the presence of some MNPs between BCP-tethered AuNPs (Supporting Information, Figure S2a). High-angle annular dark-field scanning transmission electron microscopy (HAADF-STEM; Supporting Information, Figure S5) and energy dispersive X-ray spectroscopy (EDS) showed that Fe was distributed on the entire vesicular membrane and Au was only observed in one half of both vesicles (Figure 2c,d). Hemispherical JVs had a bowl-like vesicular body containing a mixture of BCP-tethered AuNPs and MNPs, covered by a flat polymeric membrane containing MNPs only (Figure 2b). In HVs, BCP-tethered AuNPs and MNPs were distributed in the entire polymeric membrane of the HVs (Supporting Information, Figure S3).

We systematically investigated the effect of the size of BCP-tethered AuNPs (or AuNP cores), and mass fraction of MNPs in the mixed building blocks, on the assembly morphology (described in the Supporting Information). The results are summarized in a

phase-like diagram (Figure 2e). A transition from a spherical to hemispherical vesicle shape was observed when the mass fraction of MNPs in the mixed building blocks increased. We presume that the structural transition is a result of phase separation between BCP-tethered AuNPs and free PS-*b*-PAA, and the increase in packing parameter of PS-*b*-PAA upon addition of MNPs.[9,11]

The organization of both NPs in the vesicular membranes influences the optical and magnetic properties of hybrid vesicles. For the 50 nm AuNP system, the hemispherical JVs showed an increased shift in the 543 nm absorption of individual NPs to a broad peak in the range of 600 to 700 nm (Figure 3a), which was slightly more than that for spherical JVs. The red-shift in the plasmon peak is proportional to $e^{(-d/D)}$ (interparticle distance (d), NP diameter (D)).[4d,12] Thus, the larger red-shift for hemispherical JVs compared to spherical JVs can be attributed to the denser packing of AuNPs in the vesicular membrane.

We compared the r_2 of spherical and hemispherical JVs containing 50 nm AuNPs and 15 nm MNPs with that of single MNPs.[13] The r_2 of hemispherical JVs was measured from transverse relaxation (T_2)-weighted MR images (Figure 3b inset) and was calculated to be 239.6 $s^{-1}mM^{-1}$. The value was substantially higher than that for spherical JVs (114.5 $s^{-1}mM^{-1}$) and single MNPs (47.8 $s^{-1}mM^{-1}$; Figure 3b). The drastic increase in r_2 value can be attributed to the increased number of MNPs in individual hemispherical JVs compared with spherical JVs. A similar trend in r_2 increase with increasing Fe concentration was also observed with 20 nm AuNPs (Supporting Information, Figure S10).

The magnetic manipulation of JVs can enrich the materials at a target location and hence drastically enhance the localized photothermal (PT) heating. As a demonstration, we compared the increase of localized temperature before and after applying a magnetic field at one spot of the JV solution in a capillary tube when the solution was irradiated with a laser (655 nm, 0.35 Wcm^{-2}). The localized temperature of the vesicle solution increased in 4.5 min, from 24 to 40°C before magnetic concentration, and to 70°C after magnetic concentration (Figure 3c). The faster temperature increase for the group with an applied magnetic field was ascribed to more rapid heating as a result of the higher concentration of locally enriched Au materials and relatively slow heat dissipation to surrounding water.

To demonstrate the potential use of JVs in remote-controlled release of payloads, we encapsulated a model drug, fluorescein isothiocyanate (FITC), in the JVs during the assembly process. The localized PT heating melted the AuNPs and broke the integrity of the vesicles, leading to the release of payload (Supporting Information, Figure S14). Figure 3d shows that the fluorescence intensity at 520 nm increased almost linearly as a function of irradiation time and reached a plateau in 45 min (Supporting Information, Figure S15). When an external magnetic field was applied to concentrate the vesicles, the release rate of FITC from the vesicles drastically increased under the same laser irradiation (Figure 3d). By controlling the light source, a more sustained release over a longer period was achieved.

With encouraging in vitro results in hand, we evaluated the use of magneto-plasmonic JVs as contrast agents for in vivo bimodal PA and MR imaging. Hemispherical JVs containing 50 nm AuNPs and 15 nm MNPs were chosen because of their stronger plasmonic coupling

(Supporting Information, Figures S16 and S17) and administrated intravenously into athymic nude mice bearing U87MG tumors on the hind leg. In the experimental group, a magnet was attached to the hind leg of tumor-bearing mice that were intravenously injected with hemispherical JVs (the total amount of AuNPs and MNPs of injected JVs was 160.0 μg and 20.0 μg, respectively), while the control group was identical to the experimental group, but without application of a magnetic field. The tumors were imaged by PA and MR techniques before and 2 h after injection of the JVs. In the presence of a magnet, a significant darkening (49.3% from the baseline) of the tumor was observed when compared to the T_2-weight contrast images of tumors obtained before and 2 h after injection of JVs (Figure 4a,b). By contrast, in the absence of a magnet, only 18.6% darkening from the baseline was observed (Supporting Information, Figure S18). For PA imaging, the tumors were exposed to a pulsed 700 nm NIR laser, at the same value of optical density. With the assistance of an external magnetic field, the PA signals in tumors were 4.3 times greater than that before injecting JVs (Figure 4c,d; Supporting Information, Figure S19). However, without application of a magnetic field, a PA signal enhancement of only 1.9 times was observed before and after injection of JVs (Figure 4e,f; Supporting Information, Figure S19).

In summary, we successfully prepared Janus-like magneto-plasmonic hybrid vesicles with spherical and hemispherical shapes by coassembly of multiple types of building blocks. The hemispherical JVs have a strong NIR absorption and a higher r_2 than their spherical counterparts. The JVs encapsulate therapeutic compounds and the release rate of the payload can be remotely controlled by NIR light and an external magnetic field. Effective enrichment of intravenously injected JVs with an external magnetic field could drastically enhance PA and MR imaging signals in tumors. Considering the relatively large dimensions of our hybrid JVs, we are in the process of reducing their overall size to further improve pharmacokinetics and tumor-targeting ability.

Supplementary Material

Refer to Web version on PubMed Central for supplementary material.

Acknowledgments

Z.N. gratefully acknowledges the financial support of the National Science Foundation (grants: DMR-1255377, CHE-1505839) and 3M Non-tenured Faculty Award. N.M.K. and Z.N. further acknowledge support provided by a King Abdullah University of Science and Technology CRG-2015 grant. The work was also supported by the Intramural Research Program of the National Institute of Biomedical Imaging and Bioengineering, National Institutes of Health. P.H. acknowledges financial support from National Science Foundation of China (81401465, 51573096). We acknowledge Maryland NanoCenter and its NispLab. NispLab is supported, in part, by the NSF in partnership with MRSEC Shared Experimental Facilities.

References

1. a) Arvizo RR, Bhattacharyya S, Kudgus RA, Giri K, Bhattacharya R, Mukherjee P. Chem Soc Rev. 2012; 41:2943–2970. [PubMed: 22388295] b) Cobley CM, Chen J, Cho EC, Wang LV, Xia Y. Chem Soc Rev. 2011; 40:44–56. [PubMed: 20818451] c) Gao J, Gu H, Xu B. Acc Chem Res. 2009; 42:1097–1107. [PubMed: 19476332] d) Yang F, Jin C, Subedi S, Lee CL, Wang Q, Jiang Y, Li J, Di Y, Fu D. Cancer Treat Rev. 2012; 38:566–579. [PubMed: 22655679] e) Jin Y, Jia C, Huang SW, O'Donnell M, Gao X. Nat Commun. 2010; 1:41. [PubMed: 20975706] f) Lee JH, Chen KJ, Noh

SH, Garcia MA, Wang H, Lin WY, Jeong H, Kong BJ, Stout DB, Cheon J, Tseng HR. Angew Chem Int Ed. 2013; 52:4384–4388.Angew Chem. 2013; 125:4480–4484.g) Croissant J, Zink JI. J Am Chem Soc. 2012; 134:7628–7631. [PubMed: 22540671] h) Croissant J, Cattoen X, Wong Chi Man M, Durand J-O, Khashab NM. Nanoscale. 2015; 7:20318–20334. [PubMed: 26585498]

2. a) Wang L, Xu L, Kuang H, Xu C, Kotov NA. Acc Chem Res. 2012; 45:1916–1926. [PubMed: 22449243] b) Chou LYT, Zagorovsky K, Chan WCW. Nat Nanotechnol. 2014; 9:148–155. [PubMed: 24463361] c) Sánchez-Iglesias A, Grzelczak M, Altantzis T, Goris B, Pérez-Juste J, Bals S, Van Tendeloo G, Donaldson SH, Chmelka BF, Israelachvili JN, Liz-Marzán LM. ACS Nano. 2012; 6:11059–11065. [PubMed: 23186074] d) Nie Z, Fava D, Kumacheva E, Zou S, Walker GC, Rubinstein M. Nat Mater. 2007; 6:609–614. [PubMed: 17618291] e) Gao B, Arya G, Tao AR. Nat Nanotechnol. 2012; 7:433–437. [PubMed: 22683842] f) Ling D, Park W, Park S-j, Lu Y, Kim KS, Hackett MJ, Kim BH, Yim H, Jeon YS, Na K, Hyeon T. J Am Chem Soc. 2014; 136:5647–5655. [PubMed: 24689550]
3. a) Liu Y, He J, Yang K, Yi C, Liu Y, Nie L, Khashab NM, Chen X, Nie Z. Angew Chem Int Ed. 2015; 54:15809–15812.Angew Chem. 2015; 127:16035–16038.b) Huang P, Lin J, Li W, Rong P, Wang Z, Wang S, Wang X, Sun X, Aronova M, Niu G, Leapman RD, Nie Z, Chen X. Angew Chem Int Ed. 2013; 52:13958–13964.Angew Chem. 2013; 125:14208–14214.c) Song J, Zhou J, Duan H. J Am Chem Soc. 2012; 134:13458–13469. [PubMed: 22831389] d) He J, Huang X, Li Y, Liu Y, Babu T, Aronova MA, Wang S, Lu Z, Chen X, Nie Z. J Am Chem Soc. 2013; 135:7974–7984. [PubMed: 23642094] e) Lin J, Wang S, Huang P, Wang Z, Chen S, Niu G, Li W, He J, Cui D, Lu G, Chen X, Nie Z. ACS Nano. 2013; 7:5320–5329. [PubMed: 23721576] f) He J, Zhang P, Babu T, Liu Y, Gong J, Nie Z. Chem Commun. 2013; 49:576–578.
4. a) Ai H, Flask C, Weinberg B, Shuai X, Pagel MD, Farrell D, Duerk J, Gao JM. Adv Mater. 2005; 17:1949–1952.b) Ortega RA, Giorgio TD. J Nanopart Res. 2012; 14:1282.c) Schmidtke C, Eggers R, Zierold R, Feld A, Kloust H, Wolter C, Ostermann J, Merkl JP, Schotten T, Nielsch K, Weller H. Langmuir. 2014; 30:11190–11196. [PubMed: 25152249] d) Lee N, Hyeon T. Chem Soc Rev. 2012; 41:2575–2589. [PubMed: 22138852] e) Tassa C, Shaw SY, Weissleder R. Acc Chem Res. 2011; 44:842–852. [PubMed: 21661727] f) Hickey RJ, Haynes AS, Kikkawa JM, Park SJ. J Am Chem Soc. 2011; 133:1517–1525. [PubMed: 21208004]
5. a) Li Z, Yin S, Cheng L, Yang K, Li Y, Liu Z. Adv Funct Mater. 2014; 24:2312–2321.b) Todd T, Zhen Z, Tang W, Chen H, Wang G, Chuang YJ, Deaton K, Pan Z, Xie J. Nanoscale. 2014; 6:2073–2076. [PubMed: 24424277] c) Marie H, Lemaire L, Franconi F, Lajnef S, Frapart YM, Nicolas V, Frébourg G, Trichet M, Ménager C, Lesieur S. Adv Funct Mater. 2015; 25:1258–1269.d) Wang C, Sun X, Cheng L, Yin S, Yang G, Li Y, Liu Z. Adv Mater. 2014; 26:4794–4802. [PubMed: 24838472]
6. Wu C-H, Cook J, Emelianov S, Sokolov K. Adv Funct Mater. 2014; 24:6862–6871.
7. Park J, An K, Hwang Y, Park J-G, Noh H-J, Kim J-Y, Park J-H, Hwang N-M, Hyeon T. Nat Mater. 2004; 3:891–895. [PubMed: 15568032]
8. Liu Y, Li Y, He J, Duelge KJ, Lu Z, Nie Z. J Am Chem Soc. 2014; 136:2602–2610. [PubMed: 24447129]
9. Azzam T, Eisenberg A. Langmuir. 2010; 26:10513–10523. [PubMed: 20443619]
10. Hickey RJ, Koski J, Meng X, Riggleman RA, Zhang P, Park S-J. ACS Nano. 2013; 8:495–502.
11. Jain PK, Huang W, El-Sayed MA. Nano Lett. 2007; 7:2080–2088.
12. a) Lee N, Choi Y, Lee Y, Park M, Moon WK, Choi SH, Hyeon T. Nano Lett. 2012; 12:3127–3131. [PubMed: 22575047] b) Hickey RJ, Meng X, Zhang P, Park SJ. ACS Nano. 2013; 7:5824–5833. [PubMed: 23731021] c) Pöselt E, Kloust H, Tromsdorf U, Janschel M, Hahn C, Maßlo C, Weller H. ACS Nano. 2012; 6:1619–1624. [PubMed: 22276942] d) Yoon TJ, Lee H, Shao H, Hilderbrand SA, Weissleder R. Adv Mater. 2011; 23:4793–4797. [PubMed: 21953810]
13. a) Na HB, Song IC, Hyeon T. Adv Mater. 2009; 21:2133–2148.b) De La Zerda A, Zavaleta C, Keren S, Vaithilingam S, Bodapati S, Liu Z, Levi J, Smith BR, Ma TJ, Oralkan O, Cheng Z, Chen X, Dai H, Khuri-Yakub BT, Gambhir SS. Nat Nanotechnol. 2008; 3:557–562. [PubMed: 18772918]

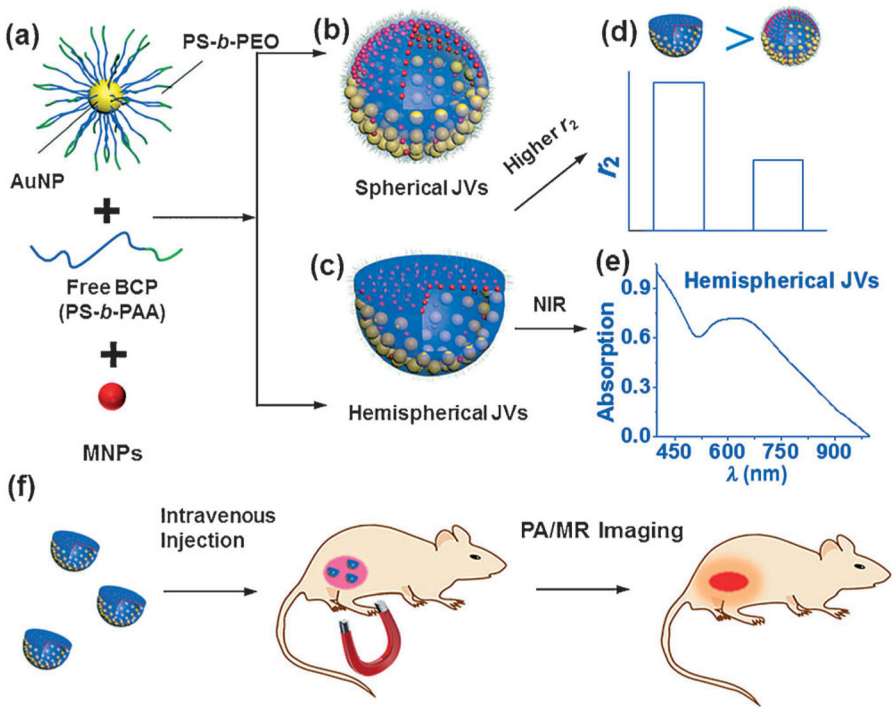

Figure 1.

a) Self-assembly of a ternary mixture of MNPs, and free BCPs of PS-*β*-PAA and PS-*β*-PEO-tethered AuNPs into hybrid JVs with different morphologies: b) spherical JVs and c) hemispherical JVs. d) Hemispherical JVs exhibit a higher transverse relaxivity (r_2) than spherical JVs and e) stronger NIR absorption. f) External magnetic field-enhanced MR and PA imaging of a tumor after intravenous injection of hemispherical JVs.

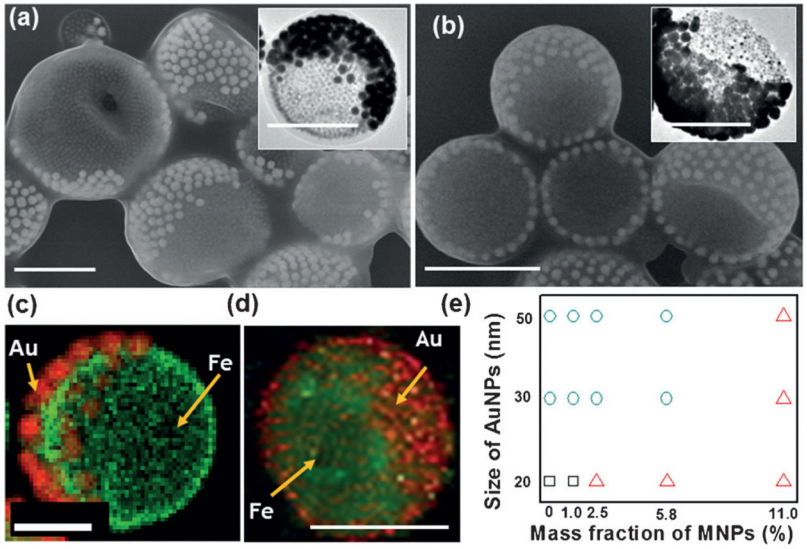

Figure 2.

SEM and TEM (inset) images of magneto-plasmonic JVs with a) spherical and b) hemispherical shapes. The mass fraction of MNPs (25 nm) used in self-assembly was 5.8 wt % (a) and 11.0 wt% (b). EDS mapping of Fe (green) and Au (red) of the c) spherical and d) hemispherical JVs. Scale bars: 500 nm (a,b), 200 nm (c), and 300 nm (d). e) Phase-like diagram of the formation of hybrid vesicles with different morphologies attained by variation of the core size of BCP-tethered AuNPs and mass fraction of MNPs. Key: spherical HVs (□), spherical JVs (○), and hemispherical JVs (△).

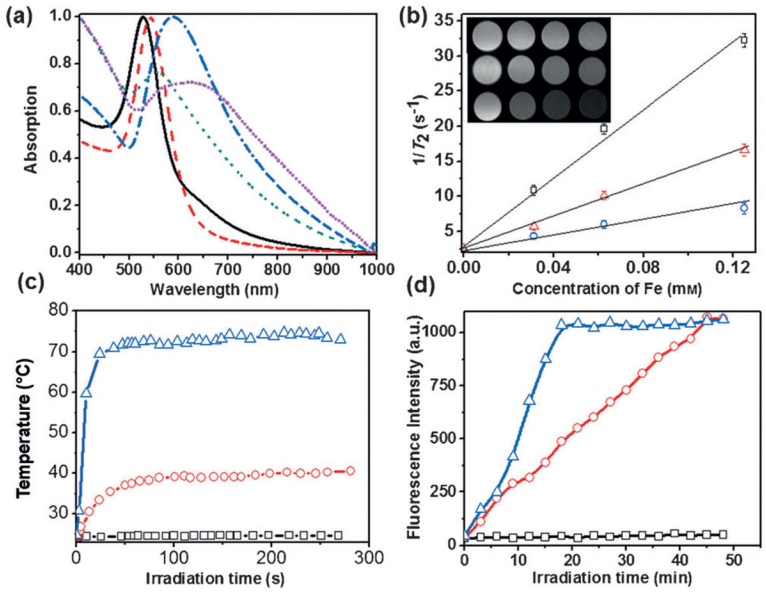

Figure 3.

a) UV/Vis absorption spectra of 20 nm AuNP (——), 50 nm AuNPs (– – –), spherical JVs with 50 nm AuNPs (–•–•–), hemispherical JVs with 50 nm AuNPs (-----) and hemispherical JVs with 20 nm AuNPs (•••••). b) Plots of r_2 value of single 15 nm MNPs (□), spherical JVs (△) and hemispherical JVs (○) composed of 50 nm AuNPs and 15 nm MNPs. The initial mass fractions of MNPs used in the assembly process were: 2.5 wt% for spherical JVs and 11.0 wt % for hemispherical JVs. The corresponding T_2-weighted images in the inset are: single MNPs, spherical JVs, and hemispherical JVs (from top to bottom). Concentrations of Fe are: 0, 0.031, 0.063, and 0.125 mM (from left to right). c) Photothermal heating induced a localized increase in the temperature of water (□), and JVs before (○) and after (△) concentration by a magnetic field. d) The FITC release profile from JVs before (○) and after (△) concentration by a magnetic field upon laser irradiation and from JVs without laser irradiation (□).

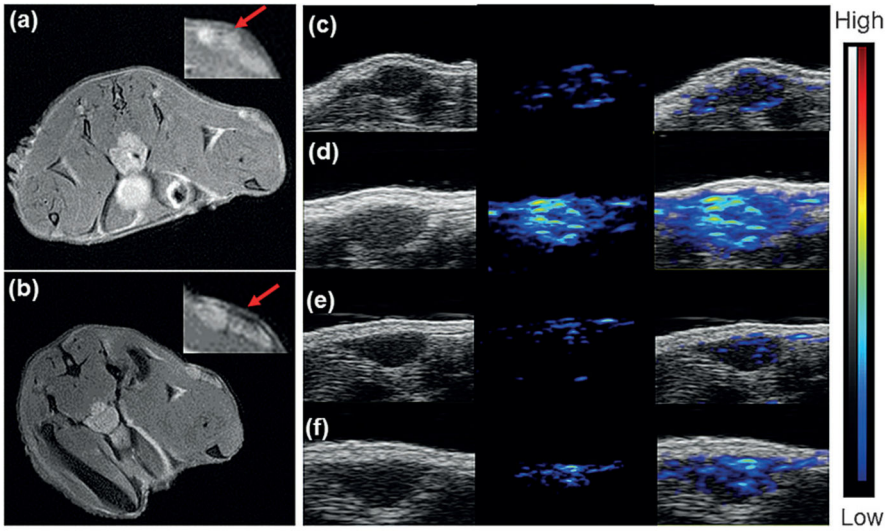

Figure 4.

a,b) In vivo MR images of athymic nude mice bearing U87MG tumors on the hind leg and corresponding tumor area (insets) before (a) and after (b) intravenous injection of hemispherical JVs containing 50 nm AuNPs and 15 nm MNPs, when a magnet is applied to the tumor. Red arrows indicate a dark area in the tumor before and after the injection. c–f) In vivo 2D ultrasonic, PA, and merged images (left to right) of tumor tissues before (c,e) and after (d,f) intravenous injection of the hemispherical JVs with (c,d) and without (e,f) a magnet attached to the leg bearing tumors.